

Deep Learning black hole metrics from shear viscosity

Yu-Kun Yan,^{1,*} Shao-Feng Wu,^{1,2,†} Xian-Hui Ge,^{1,2,‡} and Yu Tian^{3,4,5,2,§}

¹*Department of physics, Shanghai University, Shanghai, 200444, China*

²*Center for Gravitation and Cosmology, Yangzhou University, Yangzhou 225009, China*

³*School of Physics, University of Chinese Academy of Sciences, Beijing, 100049, China*

⁴*Institute of Theoretical Physics, Chinese Academy of Sciences, Beijing 100190, China*

⁵*Center for Theoretical Physics, Massachusetts Institute of Technology, MA 02139, Cambridge, USA*

Based on the AdS/CFT correspondence, we build up a deep neural network to learn the black-hole metrics from the complex frequency-dependent shear viscosity. The network architecture provides a discretized representation of the holographic renormalization group flow of the shear viscosity and is applicable for a large class of strongly coupled field theories. Given the existence of the horizon and guided by the smoothness of spacetimes, we show that the Schwarzschild and Reissner-Nordström metrics can be learned accurately. Moreover, we illustrate that the generalization ability of the deep neural network can be excellent, which indicates that using the black hole spacetime as a hidden data structure, a wide spectrum of the shear viscosity can be generated from a narrow frequency range. Our work might not only suggest a data-driven way to study holographic transports but also shed new light on the emergence mechanism of black hole spacetimes from field theories.

Introduction.—Renormalization group (RG) is a physical scheme to understand various emergent phenomena in the world through iterative coarse graining [1–4]. Deep learning (DL) algorithm is the core driving force of the recent wave of artificial intelligence [5]. It has been suggested that RG and DL might have a logic in common [6] and their relation has attracted a lot of interest [7–14]. In particular, Mehta and Schwab [15] constructed a mapping between variational RG and deep neural network (DNN) based on restricted Boltzmann machines, from which they claimed that DL algorithms may implement a generalized RG scheme.¹

RG is believed as one of the key elements to understand the quantum gravity. In particular, by anti-de Sitter/conformal field theory (AdS/CFT) correspondence [18–21], a strongly coupled quantum critical theory in the d -dimensional spacetime is reorganized along the RG scale, inducing a classical theory of gravity in the $d+1$ -dimensional AdS spacetime. RG is not the only connection between DL and gravity. Through the study of tensor networks [22–24], especially the multi-scale entanglement renormalization ansatz (MERA) [25], it has been realized that how the geometry is emergent from field theories usually involves the network and optimization, which are two important ingredients of DL.

Based on these connections, DNN is capable of providing a research platform for holographic duality [26–33]. One can expect two benefits at least: it is helpful to understand how the spacetime emerges and a data-driven phenomenological model can be built up for strongly coupled field theories. Work in the second respect was initi-

ated by [28], where the inverse problem of the AdS/CFT is studied: how to reconstruct the spacetime metric from the given field theory data by the DNN which implements the AdS/CFT. Subsequently, the so called AdS/DL correspondence is applied to learn the bulk metric from the lattice QCD data of the finite-temperature chiral condensate. Interestingly, the emergent metric exhibits both a black hole horizon and an IR wall with finite height, signaling the crossover of the QCD thermal phases [29].

In the prototype of the AdS/DL (i.e. the first numerical experiment in [28]), the architecture of the DNN is according to the discretized equation of motion of the real ϕ^4 theory minimally coupled to the gravity², the data is the one-point function and the conjugate source with a label determined by the near-horizon scale field, the target is the metric of the Schwarzschild black hole, a key technique is to design the regularization by which the learned metric is favored to be smooth, and the DNN performs better near the boundary than near the horizon where the relative error is around 30%. In [33], it has been attempted to learn the Reissner-Nordström (RN) metric by AdS/DL but the mean square error (MSE) lies in the range from $\mathcal{O}(10^{-3})$ to $\mathcal{O}(10^{-1})$. Importantly, it is revealed that the form of the regularization term must be fine-tuned for different metrics. This suggests that the DNN cannot find the target metric if it is unknown previously, because one cannot judge which is closer to the target metric under different regularizations.

In this letter, we will address the technical problems and extend the physical range of AdS/DL. We also hope to look for the insights on the emergence mechanism of spacetimes. Our strategies are as follows. First of all, consider that AdS/CFT is almost

¹ Later, it was pointed out that the standard renormalization process is essentially the feature extraction by supervised learning but cannot be generated by a general unsupervised learning unless the network structure or the loss function is designed specifically [16, 17].

² Notably, the gravity theory can be general since the scale field is assumed as a probe.

customized for the computation of the transports of strongly coupled quantum critical systems at finite temperatures [34] and in particular, the application of holography is anchored partially in the calculation of the shear viscosity [35]. Thereby we will adapt the complex frequency-dependent shear viscosity as the given field theory data. Second, we propose to build up the DNN according to the holographic RG flow of the shear viscosity. Up to the holographic renormalization, this flow was presented in the well-known holographic membrane paradigm [36, 37], which interpolates the standard AdS/CFT correspondence and classical black hole membrane paradigm smoothly [38, 39]. Third, our goal is to learn the black hole metric accurately. By selecting suitable coordinates, the metric at the horizon can be fixed as zero. This will reduce the learning difficulties. Fourth, the system error in [28] comes from adding labels artificially on the data and introducing the regularization. Because the horizon value of the shear response is completely determined by the regularity analysis at horizon, we can transfer the data from IR to UV, which is contrary to [28, 29]. Thus, our DNN can implement a generative algorithm and the data are not labeled artificially. Fifth, we still use the regularization to guide the network finding a smooth metric. However, our training process has two stages and the regularization is only required in the first stage. So we can choose any regularization term as long as it can induce a smaller loss in the second stage. Finally, we will discuss possible extensions and physical implications.

From RG flow to DNN.—Suppose that a strongly coupled field theory is dual to the 3+1-dimensional classical Einstein gravity minimally coupled with the matter, which allows a homogeneous and isotropic (along the field theory directions) black-hole solution with the metric ansatz

$$ds^2 = -g_{tt}(r)dt^2 + g_{rr}(r)dr^2 + g_{xx}(r)d\vec{x}^2, \quad (1)$$

When the black-hole background is perturbed by time-dependent sources, the shear mode $(\delta g)_{x_2}^{x_1} = h(r)e^{-i\omega t}$ of the gravitational wave is controlled by the equation of motion

$$\frac{1}{\sqrt{-g}}\partial_r(\sqrt{-g}g^{rr}\partial_r h) + g^{tt}\omega^2 h = 0, \quad (2)$$

provided that the graviton is massless [40]. In the Hamiltonian form, it can be written as

$$\Pi = -\sqrt{-g}g^{rr}\partial_r h, \quad (3)$$

$$\partial_r \Pi = \sqrt{-g}g^{rr}g^{tt}\omega^2 h, \quad (4)$$

where Π is the momentum conjugate to the field h . Consider the foliation in the r -direction and define the shear response function on each cutoff surface

$$\chi = \frac{\Pi}{i\omega h}. \quad (5)$$

Substituting Eq. (3) into Eq. (4), one can obtain a flow equation

$$\partial_r \chi - i\omega \sqrt{\frac{g_{rr}}{g_{tt}}} \left(\frac{\chi^2}{g_{xx}} - g_{xx} \right) = 0. \quad (6)$$

Note that this equation has been derived in [36] where the DC limit is focused on³. We will study the frequency-dependent behavior.

Applying the regularity of χ on the horizon, one can read off the horizon value of χ directly

$$\chi(r_h) = g_{xx}(r_h), \quad (7)$$

where r_h is the horizon radius. Taking Eq. (7) as the IR boundary condition, the flow equation can be integrated to the UV. However, it should be pointed out that the response function χ on the UV boundary is not equal to the shear viscosity η of the boundary field theory. In the Supplementary Material (SM), we will clarify the relationship between them using the Kubo formula of the complex frequency-dependent shear viscosity [44, 45] and the holographic renormalization [46]. For some holographic models, such as the Einstein-Maxwell theory that we will be concerned with, the relationship is

$$\eta(\omega) = \chi(\omega, r) + i\omega r|_{r \rightarrow \infty}. \quad (8)$$

In the metric ansatz (1), g_{xx} can be fixed as r^2 without loss of generality but g_{tt} is independent with g_{rr} in general. However, there are some black holes which share the feature $g_{tt}g_{rr} = 1$, indicating that the radial pressure is the negative of the energy density [47]. For simplicity, we will study this situation at first and return to the more general case latter. For the simple situation, the metric ansatz can be reduced to

$$ds^2 = \frac{1}{z^2} \left[-f(z)dt^2 + \frac{1}{f(z)}dz^2 + d\vec{x}^2 \right], \quad (9)$$

where we have used the coordinate $z = r_h/r$ so that the horizon is located at $z = 1$ and the boundary at $z = 0$. Accordingly, Eq. (6) can be rewritten as

$$\left(\eta - \frac{i\omega}{z} \right)' + \frac{i\omega}{f} \left[z^2 \left(\eta - \frac{i\omega}{z} \right)^2 - \frac{1}{z^2} \right] = 0, \quad (10)$$

where we have set $r_h = 1$ and the prime denotes the derivative with respect to z . Note that we have replaced $\chi(\omega, z)$ with $\eta(\omega, z) - i\omega/z$ from IR to UV. Compared to Eq. (8) where the replacement occurs only at UV, we have found that this technique reduces the discretized error considerably. The radially varying function $\eta(\omega, z)$

³ In the Wilsonian formulation, the flow equation can be retrieved as the β -functions of double-trace couplings [41–43].

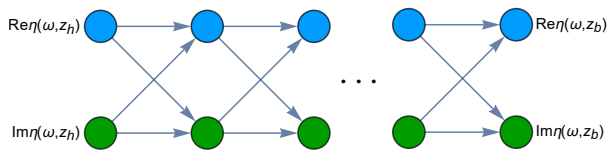


FIG. 1. The architecture of the DNN. The green and blue nodes have N layers, which upgrade the shear viscosity from IR to UV by discretized RG flow equations (12). The arrows indicate the direction of data transfer.

can be referred as the holographic RG flow of the shear viscosity. In the following, we will build up a DNN according to the flow equation (10).

A schematic diagram of the DNN is plotted in FIG. 1. The N deep layers are located by discretizing the radial direction

$$z(n) = z_b + n\Delta z, \quad \Delta z = \frac{z_h - z_b}{N}, \quad (11)$$

where z_b is the UV boundary, z_h is the IR boundary, and the integer n belong to $[1, N]$. The trainable weights of the network represent the discretized metrics. The input of the network is the given value $\eta(\omega, z_h)$. The output is $\eta(\omega, z_b)$. The data is transferred from the N th layer (IR) to the 1th layer (UV). The upgrade rule of the data between layers is determined by the discretized representation of Eq. (10)

$$\begin{aligned} \text{Re}\eta(z + \Delta z) &= \text{Re}\eta(z) \left[1 + \Delta z \frac{2\omega z^2}{f(z)} \left(\text{Im}\eta(z) - \frac{\omega}{z} \right) \right], \\ \text{Im}\eta(z + \Delta z) &= \text{Im}\eta(z) + \Delta z \frac{\omega z^2}{f(z)} \left[\frac{1 - f(z)}{z^4} \right. \\ &\quad \left. - (\text{Re}\eta(z))^2 + \left(\text{Im}\eta(z) - \frac{\omega}{z} \right)^2 \right]. \end{aligned} \quad (12)$$

Here we have separated the discretized flow equation into real and imaginary parts for the convenience in DL. We train this neural network to learn the mapping of frequencies to the shear viscosity on the boundary. Once training successfully, we can extract the discretized black hole metrics from the trained neural network.

The loss function we choose is the L^2 -norm

$$L_{\text{DNN}} = \sum_{\text{data}} [\eta(\omega, z_b) - \bar{\eta}(\omega, z_b)]^2, \quad (13)$$

up to a regularization term, if existed. Here η represents the input data and $\bar{\eta}$ is what the DNN generates.

We need a regularization term which can guide the DNN to find the smooth metric with the horizon. In principle, the form of the regularization term can be arbitrary as long as it can reduce the final loss. In practice, our regularization term can be specified as

$$\begin{aligned} L_{\text{REG}} &= c_1 \sum_{n=1}^{N-1} \frac{1}{z(n)^{c_2}} [f(z(n+1)) - f(z(n))]^2 \\ &\quad + c_3 [f(z(N)) - 0]^2, \end{aligned} \quad (14)$$

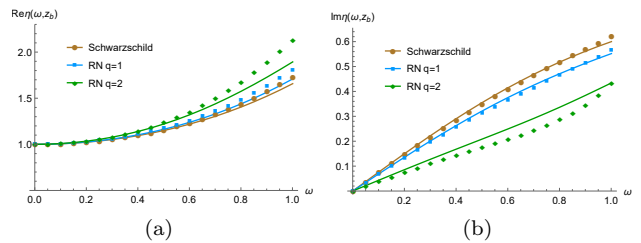


FIG. 2. The data of the shear viscosity $\eta(\omega, z_b)$ generated by Schwarzschild and RN metrics. (a) and (b) denote the real and imaginary parts, respectively. The curves are generated by the continuous holographic RG flow equation of the shear viscosity, while the markers are generated by the discretized equation.

where the two parts are designed for the smoothness of the metric and the existence of the horizon, respectively. They involve three hyperparameters c_1, c_2 and c_3 .

Data and training results.—We specify the discretized RG flow and hence the DNN by setting $z_b = 0.01$, $z_h = 0.99$, and $N = 10$. Using the discretized flow equation (12) with the IR boundary condition $\eta(\omega, z_h) = 1 + i\omega$ and the Schwarzschild metric

$$f(z) = 1 - z^3 \quad (15)$$

or the RN metric

$$f(z) = 1 - z^3 - \frac{q^2 z^3}{4} + \frac{q^2 z^4}{4} \quad (16)$$

where q is the charge density, we generate 2000 data $(\omega, \eta(\omega, z_b))$ from $\omega = 0$ to $\omega = 1$ with even spacing. The training set and validation set account for 90% and 10%, respectively. In Fig. (2), we compare the data with the ones generated by numerically solving the continuous flow equation of the shear viscosity. It is found that the discretized error is already small when the target is the Schwarzschild metric, and it increases with the frequency and the charge density. The discretized error can be reduced by adding more layers but it requires powerful computing capabilities. As a proof of principle, here we simply assume that the discretized error does not affect our results qualitatively⁴.

With the data in hand, we will train the DNN. The training scheme will be given in the SM. In TABLE S.1 of the SM, we list the training reports after two training stages of various numerical experiments. As one of the main results, it is shown that from the data with $\omega \in (0, 1]$, the Schwarzschild and RN metrics can be learned with high accuracy: the mean relative error (MRE) is

⁴ Recently, the discretized error has been taken into account for the application of AdS/DL to the QCD experimental data [48].

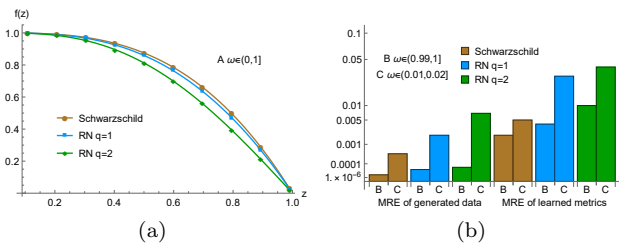


FIG. 3. The performance of the DNN. (a) The curves are the target metrics and the markers are the results learned from the data A, which has a wide frequency range. (b) The right half of the bars represents the MRE of the metrics which are learned from the data with narrow ranges B and C. The left half represents the MRE of the wideband data, which are generated using the metrics learned from the narrowband.

around $0.1\%^5$. The target and learned metrics have been plotted in FIG. (3.a).

Hereto, we almost naively select the frequency range of the data as $\Delta\omega = 1$. One important question in DL is how well does the model generalize? To proceed, we consider different datasets with the narrow frequency range $\Delta\omega = 10^{-2}$ and keep each of them with 2000 data. Interestingly, we find that both Schwarzschild and RN metrics still can be well learned, although the error will increase when the frequency window is close to zero and especially when the charge density is large. This is shown by the MRE of the metrics learned from two typical windows, see the right half of FIG. (3.b). Furthermore, it suggests that the generalization ability of the DNN can be excellent. Indeed, in the left half of FIG. (3.b), we illustrate that using the metric learned from the data with $\Delta\omega = 10^{-2}$, one can generate the data with $\Delta\omega = 1$ very accurately: in the best performing example, the MRE of the generated data can be $\mathcal{O}(10^{-6})$. We also note that the examples with relatively large errors in FIG. (3.b) can be expected because the DC limit of the shear viscosity is determined solely by the physics at horizon. Especially, when the charge density increases, the RN black hole approaches to be extremal and the IR CFT associated with the $\text{AdS}_2 \times \text{R}^2$ geometry gradually dominates the low-frequency physics [49, 50]. Similarly, we do not expect that the DNN can learn well from a very high frequency window, where the UV CFT associated with the AdS boundary should dominate⁶.

Two metric components.— A more general black hole metric has two independent metric components g_{tt} and g_{rr} . From Eq. (6), one can find that they appear in the form of the joint factor g_{rr}/g_{tt} . Therefore, the DNN can

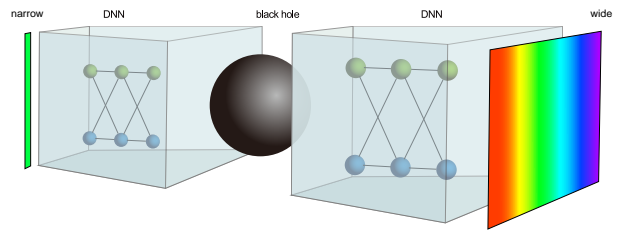


FIG. 4. Schematic diagram: the DNN encodes the black hole spacetime, by which a wide spectrum of the field theory data can be generated from its narrow piece.

be applied to learn the joint factor but in general each of them cannot be learned separately from the shear response. Nevertheless, if there are other ways to determine one, the other can be obtained by the DNN. For example, there is evidence that the entanglement plays an important role in weaving the spacetime [51–55]. Among others, it has been shown that the holographic entanglement entropy $S(l)$ can be used to fix the bulk metric wherever the extremal surface reaches [56]. Here l is the scale of the boundary entangling region on which the bulk extremal surface is anchored [52]. Under the present metric ansatz, the holographic entanglement entropy only depends on g_{rr} , so it can complement to the shear viscosity to determine two metric components.

Conclusion and discussion.—Using a simple DL method, we studied an inverse problem of AdS/CFT: given the complex frequency-dependent shear viscosity of boundary field theories at finite temperatures, whether the metrics of bulk black holes can be extracted? We showed that the Schwarzschild and RN metrics can be learned by the DNN with high accuracy. The network architecture can be taken as a discretized representation of the holographic RG flow of the shear viscosity, hence being a new application of the holographic membrane paradigm [36, 37]. We emphasize that it is applicable for a large class of strongly coupled field theories. The main limitation is that the field theory is homogeneous and isotropic, and is dual to the 3+1-dimensional Einstein gravity⁷. The extensions to the symmetry-breaking situations, the higher spacetime dimensions, and the modified theories of gravity should be plausible. Among others, we note that using the wave equation of the shear mode with the graviton mass which has been built up in [40], one can construct the RG flow and the DNN where the graviton mass is encoded into new trainable weights. It would be interesting to see whether the DNN can learn the metric and the mass simultaneously. In addition to various extensions, there are two open questions which deserve to be mentioned. (i) Is there a better ansatz for

⁵ The MSE is $\mathcal{O}(10^{-7})$.

⁶ In fact, it has been observed in [62, 63] that the retarded Green function for the shear stress operator at the infinite frequency is determined by the energy density. We thank Matteo Baggioli for the discussion on this point.

⁷ There is a subtle limitation due to the holographic renormalization, see the SM for the details.

the regularization term? Note that the regularization in this work is not to prevent overfitting as usual in machine learning. Instead, it is a guide to the minimum loss. We might need a deeper physical understanding of the regularization. (ii) How to reduce the discretized error at high frequencies and low temperatures sufficiently? Compared with directly increasing the number of layers, a more efficient method might be to apply the recently proposed DNN models of ordinary differential equations [57]. We ultimately hope that our work could suggest a data-driven way to study holographic transports.

Moreover, we found that the complete black hole metric from IR to UV can be well learned from the data with narrow frequency ranges. We also have checked that randomly deleting several data points in our numerical experiments will hardly change the performance of the DNN. These two facts indicate that the shear viscosity encodes the spacetime in a very different way from the entanglement entropy. The latter probes the deeper spacetime only by the $S(l)$ with a larger l , so any data point is necessary to reconstruct the spacetime. Perhaps we can describe this difference concisely as follows: the non-local observable (entanglement entropy) on the boundary probes the bulk spacetime locally, while the local observable (shear viscosity) probes non-locally.

Furthermore, this non-locality leads to the excellent generalization ability of the DNN, which should be important in the application to the experimental data that may be collected only in a part of the spectrum. Theoretically, from the perspective of machine learning, it usually implies that the data is highly structured⁸. This structure is often important but obscure⁹, due to the infamous black-box problem of machine learning. However, here the structure is nothing but the higher-dimensional black hole spacetime. This strong emergence might shed some lights on the understanding of DL. Last but not least, the excellent generalization suggests that the strongly coupled field theory with gravity dual could exhibit another feature of the hologram in addition to encoding the higher dimension: the local (a small piece of the hologram) can reproduce the whole, see the schematic diagram FIG. (4) for this insight.

⁸ Another possibility is that the network has some symmetry, see [58] for an example.

⁹ For example, using the generative adversarial network (GAN), the approximate statistical predictions have been made recently in the string theory landscape [59], where the accurate extrapolation capability has been exhibited on simulating Kähler metrics. It was speculated that this is the first evidence of Reid's fantasy: all Calabi-Yau manifolds with fixed dimension are connected.

Acknowledgments.—We thank Koji Hashimoto for reading the draft and giving valuable comments. We also thank Matteo Baggioli, Yongcheng Ding, Wei-Jia Li, Tomi Ohtsuki, and Fu-Wen Shu for helpful discussions. SFW and XHG are supported by NSFC grants No. 11675097 and No. 11875184, respectively. YT is supported partially by NSFC grants No. 11975235 and No. 11675015. He is also supported by the “Strategic Priority Research Program of the Chinese Academy of Sciences” with Grant No. XDB23030000.

* ykyan.phys@gmail.com

† sfwu@shu.edu.cn

‡ gexh@shu.edu.cn

§ ytian@ucas.ac.cn

- [1] K. G. Wilson and J. Kogut, Phys. Rep. **12**, 75 (1974).
- [2] K. G. Wilson, Rev. Mod. Phys. **55**, 583 (1983).
- [3] J. Polchinski, Nucl. Phys. B **231**, 269 (1984).
- [4] L. P. Kadanoff, Physics Physique Fizika **2**, 263 (1966).
- [5] T. J. Sejnowski, The Deep Learning Revolution, The MIT Press, 2018.
- [6] X. G. Wen, <http://url.cn/5eKhBBP>. (In Chinese)
- [7] C. Bény, arXiv:1301.3124.
- [8] S. Saremi and T. J. Sejnowski, PNAS **110**, 3071 (2013).
- [9] A. Paul and S. Venkatasubramanian, arXiv:1412.6621.
- [10] S. Braddeea and W. Bialek, J. Stat. Phys. **167**, 462 (2017) arXiv:1610.09733.
- [11] D. Oprisa and P. Toth, arXiv:1705.11023.
- [12] S. Foreman, J. Giedt, Y. Meurice, and J. Unmuth-Yockey, EPJ. Web. Conf. **175**, 11025 (2018) arXiv:1710.02079.
- [13] S. Iso, S. Shibaa and S. Yokoo, Phys. Rev. E **97**, 053304 (2018) arXiv:1801.07172
- [14] S. H. Li and L. Wang, Phys. Rev. Lett. **121**, 260601 (2018) arXiv:1802.02840
- [15] P. Mehta and D. J. Schwab, arXiv:1410.3831.
- [16] H. W. Lin, M. Tegmark, and D. Rolnick, J. Stat. Phys. **168**, 1223-1247 (2017) arXiv:1608.08225.
- [17] M. Koch-Janusz and Z. Ringel, Nature. Phys. **14**, 578 (2018) arXiv:1704.06279; P. M. Lenggenhager, Z. Ringel, S. D. Huber, and M. Koch-Janusz, Phys. Rev. X **10**, 011037 (2020) arXiv:1809.09632.
- [18] J. M. Maldacena, Adv. Theor. Math. Phys. **2**, 231 (1998) arXiv:hep-th/9711200.
- [19] S. S. Gubser, I. R. Klebanov, and A. M. Polyakov, Phys. Lett. B **428**, 105 (1998) arXiv:hep-th/9802109.
- [20] E. Witten, Adv. Theor. Math. Phys. **2**, 253 (1998) arXiv:hep-th/9802150.
- [21] L. Susskind and E. Witten, arXiv:hep-th/9805114.
- [22] J. C. Bridgeman and C. T. Chubb, J. Phys. A: Math. Theor. **50**, 223001 (2017) arXiv:1603.03039.
- [23] U. Schollwöck, Ann. Phys. **326**, 96-192 (2011) arXiv:1008.3477.
- [24] G. Evenbly and G. Vidal, J. Stat. Phys. **145**, 891 (2011) arXiv:1106.1082.
- [25] G. Vidal, Phys. Rev. Lett. **99**, 220405 (2007) arXiv:condmat/0512165; G. Vidal, Phys. Rev. Lett. **101**, 110501 (2008) arXiv:quant-ph/0610099; G. Evenbly and G. Vidal, Phys. Rev. B **79**, 144108 (2009) arXiv:0707.1454.

- [26] W. C. Gan and F. W. Shu, *Int. J. Mod. Phys. D* **26**, 1743020 (2017), arXiv:1705.05750.
- [27] Y.-Z. You, Z. Yang, and X.-L. Qi, *Phys. Rev. B* **97**, 045153 (2018) arXiv:1709.01223.
- [28] K. Hashimoto, S. Sugishita, A. Tanaka, and A. Tomiya, *Phys. Rev. D* **98**, 046019 (2018) arXiv:1802.08313.
- [29] K. Hashimoto, S. Sugishita, A. Tanaka, and A. Tomiya, *Phys. Rev. D* **98**, 106014 (2018) arXiv:1809.10536.
- [30] K. Hashimoto, *Phys. Rev. D* **99**, 106017 (2019) arXiv:1903.04951.
- [31] H. Y. Hu, S. H. Li, L. Wang, and Y. Z. You, arXiv:1903.00804
- [32] X. Han and S. A. Hartnoll, *Phys. Rev. X* **10**, 011069 (2020) arXiv:1906.08781.
- [33] J. Tan and C. B. Chen, *Int. J. Mod. Phys. D* **28**, 1950153 (2019) arXiv:1908.01470.
- [34] J. Zaanen, Y. W. Sun, and Y. Liu, *Holographic duality in condensed matter physics*, (CUP, 2015), Section 7.
- [35] P. Kovtun, D. T. Son and A. O. Starinets, *Phys. Rev. Lett.* **94**, 111601 (2005) arXiv:hep-th/0405231.
- [36] N. Iqbal and Hong Liu, *Phys. Rev. D* **79**, 025023 (2009) arXiv:0809.3808.
- [37] I. Bredberg, C. Keeler, V. Lysov, and A. Strominger, *JHEP* **1103**, 141 (2011) arXiv:1006.1902.
- [38] K. S. Thorne, R. H. Price and D. A. Macdonald, *Black holes: the membrane paradigm*, Yale University Press, New Haven 1986.
- [39] M. Parikh and F. Wilczek, *Phys. Rev. D* **58**, 064011 (1998) arXiv:gr-qc/9712077.
- [40] S. A. Hartnoll, D. M. Ramirez, and J. E. Santos, *JHEP* **1603**, 170 (2016) arXiv:1601.02757.
- [41] D. Nickel and D. T. Son, *New. J. Phys.* **13**, 075010 (2011) arXiv:1009.3094.
- [42] I. Heemskerk and J. Polchinski, *JHEP* **06**, 031 (2011) arXiv:1010.1264.
- [43] T. Faulkner, H. Liu and M. Rangamani, *JHEP* **08**, 051 (2011) arXiv:1010.4036.
- [44] B. Bradlyn, M. Goldstein, and N. Read, *Phys. Rev. B* **86**, 245309 (2012) arXiv:1207.7021.
- [45] M. Geracie, D. T. Son, C. Wu, and S. F. Wu, *Phys. Rev. D* **91**, 045030 (2015) arXiv:1407.1252.
- [46] M. Henningson and K. Skenderis, *JHEP* **07**, 023 (1998) arXiv:hep-th/9806087; S. de Haro, S. N. Solodukhin, and K. Skenderis, *Commun. Math. Phys.* **217**, 595 (2001) arXiv:hep-th/0002230; M. Bianchi, D. Z. Freedman, and K. Skenderis, *Nucl. Phys. B* **631**, 159 (2002) arXiv:hep-th/0112119.
- [47] T. Jacobson, *Class. Quant. Grav.* **24**, 5717 (2007) arXiv:0707.3222.
- [48] T. Akutagawa, K. Hashimoto, and T. Sumimoto, arXiv:2005.02636.
- [49] T. Faulkner, H. Liu, J. McGreevy, and D. Vegh, *Phys. Rev. D* **83**, 125002 (2011) arXiv:0907.2694.
- [50] M. Edalati, J. I. Jottar and R. G. Leigh, *JHEP* **1001**, 18 (2010) arXiv:0910.0645.
- [51] J. M. Maldacena, *JHEP* **04**, 021 (2003) arXiv:hep-th/0106112.
- [52] S. Ryu and T. Takayanagi, *Phys. Rev. Lett.* **96**, 181602 (2006) arXiv:hep-th/0603001.
- [53] B. Swingle, *Phys. Rev. D* **86**, 065007 (2012) arXiv:0905.1317.
- [54] M. Van Raamsdonk, *Gen. Rel. Grav.* **42**, 2323 (2010) arXiv:1005.3035.
- [55] J. Maldacena and L. Susskind, *Fortsch. Phys.* **61**, 781 (2013) arXiv:1306.0533.
- [56] S. Bilson, *JHEP* **08**, 073 (2008) arXiv:0807.3695; *JHEP* **02**, 050 (2011) arXiv:1012.1812.
- [57] R. T. Q. Chen., Y. Rubanova, J. Bettencourt, and D. Duvenaud, NIPS'18: Proceedings of the 32nd International Conference on Neural Information Processing Systems 6572-6583 (2018) arXiv:1806.07366.
- [58] C. Wang, H. Zhai, and Y. Z. You, arXiv:1901.11103.
- [59] J. Halverson and C. Long, arXiv:2001.00555.
- [60] J. Schwinger, *J. Math. Phys.* **2**, 407 (1961).
- [61] See a review: K. C. Chou, Z. B. Su, B. L. Hao, and L. Yu, *Phys. Report.* **118**, 1 (1985).
- [62] T. Andrade, M. Baggioli, and O. Pujolàs, *Phys. Rev. D* **100**, 106014 (2019) arXiv:1903.02859.
- [63] M. Baggioli, S. Grienering, and H. Soltanpanahi, *Phys. Rev. Lett.* **124**, 081601 (2020) arXiv:1910.06331.
- [64] L. V. Keldysh, *Zh. Eksp. Teor. Fiz.* **47**, 1515 (1964) [*Sov. Phys. JETP* **20**, 1018 (1965)].
- [65] D. T. Son, Viscosity, Black Holes, and Relativistic Heavy Ion Collisions, Physics/Applied Physics colloquium at Stanford University, 2007.
- [66] T. Tieleman and G. Hinton. Lecture 6.5—RmsProp: Divide the gradient by a running average of its recent magnitude. COURSERA: Neural Networks for Machine Learning, 2012.
- [67] D. Kingma and J. Ba: Adam: arXiv:1412.6980.
- [68] R. Iten, T. Metger, H. Wilming, L. D. Rio, and R. Renner, *Phys. Rev. Lett.* **124**, 010508 (2020) arXiv:1807.10300.

Supplementary material for 'Deep Learning black hole metrics from shear viscosity'

COMPLEX FREQUENCY-DEPENDENT SHEAR VISCOSITY

Compared to the real shear viscosity at the zero frequency limit, the study of complex frequency-dependent counterparts is rare. So let's begin from reviewing the Kubo formula of the complex frequency-dependent shear viscosity. In [44], the Kubo formulas for the stress-stress response function at zero wavevector is derived from first principles. The approach given in [44] starts from a microscopic Hamiltonian and define the viscosity tensor as the linear response to a uniform external strain. In [45], an alternative field-theory approach is proposed, by which the Ward identity of viscosity coefficients in [44] is retrieved and extended. Here we will follow [45] to give the definition of the complex frequency-dependent shear viscosity by the generating functional.

For a theorist, the viscosity can be measured by sending a gravitational wave through the system [65]. Suppose that a homogeneous and isotropic system lives in the two-dimensional flat space which is perturbed by a uniform gravitational wave. The response tensor Y^{ijkl} can be defined by

$$\delta\langle T^{ij}(t)\rangle_r = -\frac{1}{2} \int dt' Y^{ijkl}(t-t') \partial_{t'} \delta g_{rkl}(t'), \quad (\text{S.1})$$

Here the subscript r and the subscript a below indicate that we have invoked the closed time-path formalism to discuss the real-time response [60, 61, 64]. The elastic modulus and the viscosity tensor can be further defined by separating the right hand of Eq. (S.1) into two parts,

$$\delta\langle T^{ij}(t)\rangle_r = -\frac{1}{2} \int dt' \lambda^{ijkl}(t-t') \delta g_{rkl}(t') - \frac{1}{2} \int dt' \eta^{ijkl}(t-t') \partial_{t'} \delta g_{rkl}(t'). \quad (\text{S.2})$$

The stress tensor can be derived by the variation of the generating functional with respect to the metric

$$\langle T^{ij}(t)\rangle_r = \frac{2}{\sqrt{g}} \frac{\delta W}{\delta g_{aij}(t)}, \quad (\text{S.3})$$

and the second variation leads to the retarded correlator

$$G_{ra}^{ij,kl}(t) \equiv \frac{4\delta W}{\delta g_{aij}(t) \delta g_{rkl}(0)} = \delta^{kl} \langle T^{ij} \rangle \delta(t) - \lambda^{ijkl}(t) - \partial_t \eta^{ijkl}(t). \quad (\text{S.4})$$

The elastic modulus is the stress response up to the zeroth-order in time derivatives, which can be determined by the constitute relation of perfect fluids. In hydrodynamic expansion, one has

$$\delta\langle T^{ij}(t)\rangle_r = - \left(P \delta^{ik} \delta^{jl} + \frac{1}{2} \delta^{ij} \delta^{kl} \kappa^{-1} \right) \delta g_{rkl}(t), \quad (\text{S.5})$$

where P is the pressure and κ^{-1} is the inverse compressibility. Then the elastic modulus can be given by

$$\lambda^{ijkl}(t) = [P (\delta^{ik} \delta^{jl} + \delta^{il} \delta^{jk}) + \delta^{ij} \delta^{kl} \kappa^{-1}] \delta(t). \quad (\text{S.6})$$

The viscosity tensor can be decomposed as

$$\eta^{ijkl}(t) = \zeta(t) \delta^{ij} \delta^{kl} + \eta(t) (\delta^{ik} \delta^{jl} + \delta^{il} \delta^{jk} - \delta^{ij} \delta^{kl}) + \eta^H(t) (\delta^{jk} \epsilon^{il} - \delta^{il} \epsilon^{kj}). \quad (\text{S.7})$$

The coefficients ζ, η, η^H denote the bulk, shear, and Hall viscosities, respectively. Substituting the last two equations into Eq. (S.4), one can obtain

$$\begin{aligned} G_{ra}^{12,12}(t) &= -\lambda^{1212}(t) - \partial_t \eta^{1212}(t) \\ &= -P \delta(t) - \partial_t \eta(t). \end{aligned} \quad (\text{S.8})$$

In Fourier space, we have the Kubo formula of the shear viscosity

$$\eta(\omega) = \frac{G_{ra}^{12,12}(\omega) + P}{i\omega}. \quad (\text{S.9})$$

Note that this formula applies to the complex shear viscosity at all frequencies. In contrast, many literatures focus on the real part and the DC limit of the shear viscosity, so the pressure in Eq. (S.9) is often neglected.

HOLOGRAPHIC RENORMALIZATION

We proceed to bridge the shear viscosity $\eta(\omega)$ to the shear response $\chi(\omega)$. The essential procedure is to carry out the holographic renormalization [46]. Consider that the bulk action includes the Einstein gravity and the minimally coupled matter

$$S_{\text{bulk}} = \int d^4x \sqrt{-g} (R + 6 + L_{\text{matter}}), \quad (\text{S.10})$$

where we have set the AdS radius $L = 1$ and the Newton constant $16\pi G_N = 1$. Suppose that the background metric is homogeneous and isotropic along the field theory directions

$$ds^2 = -g_{tt}(r)dt^2 + g_{rr}(r)dr^2 + g_{xx}(r)d\vec{x}^2. \quad (\text{S.11})$$

Accordingly, the energy-momentum tensor can be written by

$$T_{\mu\nu} = \text{diag}(T_{tt}(r), T_{rr}(r), T_{xx}(r), T_{xx}(r)). \quad (\text{S.12})$$

Perturbing the Einstein equation on the background, the wave equation of the shear mode is derived as [40]

$$\frac{1}{\sqrt{-g}} \partial_r (\sqrt{-g} g^{rr} \partial_r h) + g^{tt} \omega^2 h = 0, \quad (\text{S.13})$$

where we have assumed that the square of the graviton mass $m^2 = g^{xx} T_{xx} - \delta T_{xy} / \delta g_{xy}$ is vanishing. Without loss of generality, we will set $g_{xx} = r^2$ hereafter. We further require that the metric can be expanded near the AdS boundary, with the form

$$\begin{aligned} g_{tt} &= r^2 \left(1 + \frac{a_1}{r} + \frac{a_2}{r^2} + \frac{a_3}{r^3} + \dots \right), \\ g^{rr} &= r^2 \left(1 + \frac{b_1}{r} + \frac{b_2}{r^2} + \frac{b_3}{r^3} + \dots \right), \end{aligned} \quad (\text{S.14})$$

where a_i and b_i are some constants.

Near the boundary, the wave equation of the shear mode has the asymptotic solution

$$h = h^{(0)} + \frac{1}{r^2} h^{(2)} + \frac{1}{r^3} h^{(3)} + \dots. \quad (\text{S.15})$$

Here $h^{(0)}$ is the source, $h^{(2)}$ is fixed by $h^{(0)}$ as $h^{(2)} = h^{(0)} \omega^2 / 2$, and $h^{(3)}$ relies on $h^{(0)}$ and the incoming boundary condition at the horizon. In solving the asymptotic equation, one can find

$$(a_1 + b_1) \omega^2 h^{(0)} = 0. \quad (\text{S.16})$$

The situation $a_1 = -b_1 \neq 0$ is rare, if existed. So we focus on $a_1 = -b_1 = 0$.

We write down the Gibbons-Hawking term and the counterterms

$$S_{\text{GH}} = -2 \int d^3x \sqrt{-\gamma} K, \quad (\text{S.17})$$

$$S_{\text{ct}} = \int d^3x \sqrt{-\gamma} \left(-4 + R + L_{\text{matter}}^{(1)} \right), \quad (\text{S.18})$$

where γ^{ab} is the induced metric, K is the external curvature, and $L_{\text{matter}}^{(1)}$ is contributed by the matter.

We expand the on-shell bulk action, the Gibbons-Hawking term and the counterterms to the quadratic order of the shear mode,

$$\begin{aligned} & S_{\text{bulk}} + S_{\text{GH}} + S_{\text{ct}}|_{\text{on-shell, quadratic}} \\ &= \int d^2x \int_{-\infty}^{\infty} \frac{d\omega}{2\pi} \frac{1}{2} \left[\left(-\frac{r^2 \omega^2}{\sqrt{g_{tt}}} + 4r^2 \sqrt{g_{tt}} - 2r \sqrt{\frac{g_{tt}}{g_{rr}}} - \frac{r^2 g'_{tt}}{\sqrt{g_{tt} g_{rr}}} + L_{\text{matter}}^{(2)} \right) \bar{h} h - r^2 \sqrt{\frac{g_{tt}}{g_{rr}}} \bar{h} h' \right], \end{aligned} \quad (\text{S.19})$$

where \bar{h} has the argument $-\omega$ and $L_{\text{matter}}^{(2)}$ denotes the matter contribution which may be divergent on the boundary.

Substituting the asymptotic solution (S.15) and the metric (S.14) into Eq. (S.19), we obtain the renormalized action:

$$S_{\text{ren}} = \int d^2x \int_{-\infty}^{\infty} \frac{d\omega}{2\pi} \frac{1}{2} \left[(3a_3 - 2b_3 + L_{\text{matter}}^{(3)}) \bar{h}^{(0)} h^{(0)} + 3\bar{h}^{(0)} h^{(3)} \right], \quad (\text{S.20})$$

where $L_{\text{matter}}^{(3)}$ is contributed by the matter and it is finite.

Invoking the holographic dictionary, one can extract the retarded correlator from S_{ren} :

$$G_{\text{ra}}^{12,12}(\omega) = (3a_3 - 2b_3 + L_{\text{matter}}^{(3)}) + 3 \frac{h^{(3)}}{h^{(0)}}. \quad (\text{S.21})$$

Expand the response function near the boundary

$$\chi \equiv \frac{\Pi}{i\omega h} = -\frac{\sqrt{-g}g^{rr}\partial_r h}{i\omega h} = \frac{3}{i\omega} \frac{h^{(3)}}{h^{(0)}} - i\omega r \Big|_{r \rightarrow \infty}. \quad (\text{S.22})$$

Then we have

$$G_{\text{ra}}^{12,12}(\omega) = (3a_3 - 2b_3 + L_{\text{matter}}^{(3)}) + i\omega (\chi + i\omega r)_{r \rightarrow \infty}. \quad (\text{S.23})$$

Reading the pressure $P = -G_{\text{ra}}^{12,12}(0)$ from Eq. (S.9) and the DC response $\chi(0) = r^2$ from Eq. (6), we find

$$G_{\text{ra}}^{12,12}(\omega) = -P + i\omega (\chi + i\omega r)_{r \rightarrow \infty} + L_{\text{matter}}^{(3)}(\omega) - L_{\text{matter}}^{(3)}(0). \quad (\text{S.24})$$

Notice that $L_{\text{matter}}^{(1)}$ should be an intrinsic scalar on the 2+1-dimensional boundary, which indicates that we can parameterize

$$L_{\text{matter}}^{(3)}(\omega) - L_{\text{matter}}^{(3)}(0) = \omega^2 M, \quad (\text{S.25})$$

where M represents a finite real number.

Combining Eq. (S.24), Eq. (S.25) and Eq. (S.9), we obtain the relationship between shear response and shear viscosity

$$\eta(\omega) = \chi(\omega) + i\omega r \Big|_{r \rightarrow \infty} - i\omega M. \quad (\text{S.26})$$

Some remarks on the parameter M are in order. First of all, for the Einstein-Maxwell theory, M is equal to zero. Second, it is also vanishing for some other matter fields. We take the massive scalar field ϕ as an example, which is dominated by

$$L_{\text{matter}} = -g^{\mu\nu} \partial_\mu \phi \partial_\nu \phi - m_\phi^2 \phi^2. \quad (\text{S.27})$$

It is dual to the relevant operator with the conformal dimension $\Delta_\phi = \frac{3}{2} + \sqrt{\frac{9}{4} + m_\phi^2}$ when $\Delta_\phi < 3$. The scalar field yields two counterterms related to ω^2 , that is

$$L_{\text{matter}}^{(1)} = \phi \nabla^2 \phi + R\phi^2, \quad (\text{S.28})$$

where we have neglected two prefactors. Since ϕ is assumed to be homogeneous and isotropic on the boundary, the former term does not contribute to M . When $\Delta_\phi < 5/2$, the latter term does not contribute either. Third, for the bottom-up holographic model, usually only the IR behavior of the metric is concerned. Instead, the holographic renormalization depends on the UV alone. Thus, one can assume that the target IR metric is embedded into a suitable UV background, by which $M = 0$. In the main text, we focus on the UV-complete metrics with $M = 0$ for simplicity. More generally, one can follow this philosophy. Finally, even if M is essential in some situations, one can replace χ with $\chi + i\omega M$, which will introduce a trainable weight in the DNN and leave a general formula

$$\eta(\omega) = \chi(\omega) + i\omega r \Big|_{r \rightarrow \infty}. \quad (\text{S.29})$$

In the future, we would like to study whether the metric still can be learned by the DNN with the additional weight.

TRAINING SCHEME AND REPORT

For all numerical experiments in this letter, we implement the same training scheme. We train the network in two stages. First, the initial weights are randomly selected from $(0, 2)$. The loss function is given by the sum of Eq. (13) and Eq. (14). We will adopt the RMSProp optimizer [66]. Second, the initial weights of the DNN will be replaced by the trained weights of the first stage. The loss function is re-set as Eq. (13) without the regularization. Then the network will be trained again with the optimizer Adam [67]. After the training of each stage, one can read the loss, extract the weights, and calculate their error. It can be found that after the second stage of training, the performance of the DNN is usually improved. In particular, the loss (without regularizations) of the first stage can be reduced by several orders of magnitude. Moreover, turning the regularization factors in the first stage can improve the performance of the DNN in the second stage. With this in mind, we will scan the parameter space of regularization factors.

In two stages of training, we fix the batch size $c_{\text{bs}} = 512$, but the learning rate is changed even not once and selected by experience. The number of epoches in each stage is large enough so that the training will not stop until the validation loss is almost not reduced. The regularization factor c_3 is set as $15c_1$. We focus on turning the regularization factors c_1 and c_2 because the performance of the DNN is more sensitive to them than other hyperparameters. Initially, c_1 and c_2 are limited to some suitable ranges. Then we scan the two-dimensional parameter space. Considering the statistical fluctuation due to the randomized initialization of the network, we train 5 times for each set of regularization factors [68]. We gradually move and reduce the ranges of parameters. We also gradually reduce the step sizes. Thus, the scanning is concentrated around the c_1 and c_2 where the DNN produces smaller losses. We stop the scanning when the step sizes $\Delta c_1 < 10^{-5}$ and $\Delta c_2 < 0.01$.

We select the optimal regularization factors as the ones according to the minimum loss. We read the minimum loss and the trained weights of the network accordingly, and then calculate the MRE of the weights and the MRE of the wideband data generated by the weights learned from narrowband data. These quantities are considered as the final performance of the DNN. We simply refer them as the ‘‘minimum loss’’, the ‘‘learned metric’’, the ‘‘MRE of learned metrics’’, and the ‘‘MRE of generated data’’, respectively. They have been exhibited in FIG. 3 of the main text and in TABLE S.1.

TABLE S.1. Training reports of various numerical experiments. We have three target metrics and each of them is learned from three datasets: A $\omega \in (0, 1]$, B $\omega \in (0.99, 1]$, and C $\omega \in (0.01, 0.02]$. We list two optimal regularization factors and three quantities which characterize the performance of the DNN.

Target	Data	Optimal c_1	Optimal c_2	Minimum loss	MRE of learned metrics	MRE of generated data
Schwarzschild	A	1.20×10^{-3}	2.02	1×10^{-13}	1×10^{-3}	/
Schwarzschild	B	1.4×10^{-4}	1.52	6×10^{-13}	2×10^{-3}	5×10^{-6}
Schwarzschild	C	3.4×10^{-4}	1.49	1×10^{-14}	5×10^{-3}	4×10^{-4}
RN q=1	A	9×10^{-5}	2.00	1×10^{-13}	1×10^{-3}	/
RN q=1	B	2.6×10^{-4}	1.30	7×10^{-13}	4×10^{-3}	3×10^{-5}
RN q=1	C	1.1×10^{-4}	0.90	1×10^{-14}	3×10^{-2}	2×10^{-3}
RN q=2	A	7×10^{-5}	1.25	1×10^{-12}	7×10^{-4}	/
RN q=2	B	6×10^{-5}	1.15	2×10^{-11}	1×10^{-2}	5×10^{-5}
RN q=2	C	4.2×10^{-4}	0.50	2×10^{-14}	4×10^{-2}	7×10^{-3}